Prediction of flow phenomena, performance and thrust forces of three-stage pump by using URANS

IOP Conf. Series: Earth and Environmental Science **240** (2019) 092003 doi:10.1088/1755-1315/240/9/092003

Prediction of flow phenomena, performance and thrust forces of three-stage pump by using URANS

Hiroyoshi Watanabe

EBARA Corporation, Fluid Machinery & Systems Company, 78-1 Shintomi, Futtu-shi, Chiba 293-0011, JAPAN
watanabe.hiroyoshi@ebara.com

Abstract. This paper describes the results of CFD prediction of performance, internal flow fields and thrust force acting on the impellers of a three-stage centrifugal pump which was provided for the Workshop "Single-&Multistage Pump Flow Prediction". URANS (Unsteady Reynolds Averaged Navier-Stokes) was applied for the CFD prediction. Parts of the results were already reported by the authors. In this paper, more details are described, especially on the relationship between the changes of the flow fields in the pump and performance of axial thrust characteristics. The effects of axial shift on the performance and axial thrust characteristic are also investigated. URANS calculations were conducted at the design flow (Q_d) to a near shut-off condition (10% Q_d). The predicted Q-H performance shows a good agreement with the experiments. This pump shows positive slope in the head curve near the shut-off condition. URANS predicted the positive slope in the head curve near the shut-off condition, its flow rate, however, was slightly higher than that of the experiment. The reverse flow between the impeller and the diffuser developed when the flow rate was reduced. The interaction between the reverse flows and the flow in the side-wall gaps (front, back) affects pressure distributions and then axial thrust acts on the impeller. The details of the change of the interaction by flow rate predicted by URANS are described including the effects of axial shift of the rotor. URANS predicted earlier change in the axial thrust characterized by axial shift of the rotor than occurred in the experiments. This discrepancy was caused by interaction between reverse flows and side wall gap flows starting at higher flow than in the experiments.

1. Introduction

High head multi-stage centrifugal pumps applied as boiler feed pumps for thermal power plants require high mechanical reliability as well as high performance. In order to improve pump performance and reliability, it is essential to clarify and understand flow phenomena in the pump at design and off-design operating conditions which induce problems.

As for pump reliability, prediction of the residual axial thrust over the whole operating range, including design and part load flow conditions is essential for proper and economical design of thrust bearings and balancing devices such as balance pistons. There are many results on predicting thrust forces acts on impellers based both on the theoretical model of side wall gap flow [1], and on experimental investigations [2]and CFD predictions [3], [4].

However, at the part load condition, the interactions between the flows at impeller exit and in the side wall gaps should be much more essential. It is known that a sudden change in axial thrust at part load operating conditions was caused by the misalignment of the axial position of the impellers[5],[6] which could be caused by the accumulation of geometrical tolerances.

As the authors reported in the previous paper [7], the interaction of the reverse flow from the diffuser and the flow in the front and back side gaps between the impeller and the casing affects the swirl velocity and pressure distributions inside the gaps. This induces the change in thrust force on the impeller, which depends on the pressure distribution in the front and back side gaps.

The paper also investigates the effects of the misalignment of the axial position of the impellers on the thrust forces on the impellers. The results showed the smaller the overlap between the impeller shroud and diffuser casing wall by the axial offsets, the greater the flow to leak out from the impeller side into the side wall gaps. The swirl flow in the gaps weakens because of the stronger interaction with the reverse flow from the diffuser.

This paper provides more details on the changes in the performance, flow field and thrust forces using URANS results on part load flow (80%,60%, 40% and 10% design flow) added to the results of design flow and 20% flow reported in the previous paper. In addition to these results, the source of the positive slope in the head curve near the shut-off condition is also described, based on changes in the flow field analyzed using URANS.

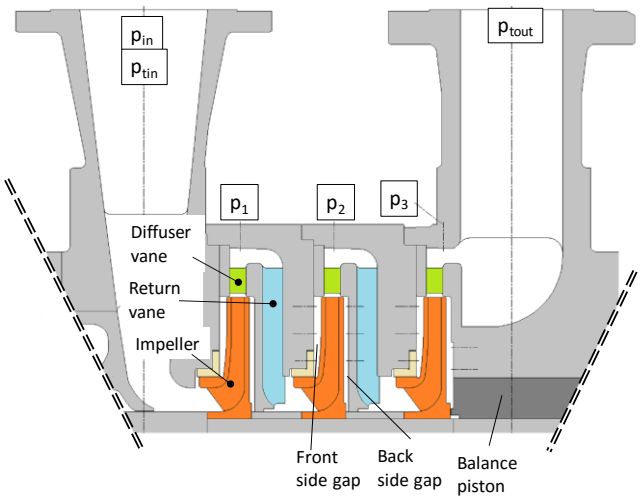

Figure 1. Three stages centrifugal pump.

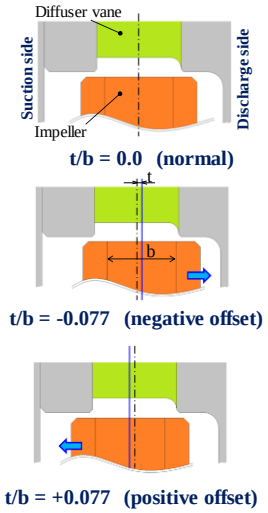

Figure 2. Axial offset of the rotor.

2. Target three-stage pump

The schematic view of the three-stage centrifugal pump is shown in figure 1., which is the target of the analysis in the Workshop. The details of the components of the pump were also described in the paper [7]. The geometry of each stage of the pump is basically identical and each stage consists of an impeller, vaned diffuser, and return channel. The third stage does not have a return channel and the diffuser directly connected to the discharge casing. The number of impeller blades is 7, and the number of diffuser vanes and return channel vane is 10. A balance piston is employed to compensate for the axial thrust forces working on the impellers. The radial clearances at the front wearing ring and inter-stage bush are 0.19 mm and 0.18 mm respectively. The radial clearance at the balance piston is 0.18 mm.

The axial offsets of the rotor position were adjusted by employing a spacer placed near the thrust bearing of the shaft. Three cases of axial offset/impeller exit height ratio were tested, as shown in figure 2. : $t/b = +0.077$ (offset to suction side), $t/b = -0.077$ (offset to discharge side) and the normal condition, $t/b = 0.0$, in which the center lines of the impeller exit width and diffuser width are at the same location.

The details of the measuring methods and the experimental results were reported by Yamashita et.al [8] and were provided in the Workshop.

3. Numerical method

The commercial Navier-Stokes code ANSYS CFX [9] was employed to analyze pump performance, detailed flow fields and axial thrust forces working on the rotor. Tetra-prism mesh was used for the suction and discharge casings; hexahedral mesh was used for the impeller, diffuser, side wall gaps and clearance sections. The total number of elements used in the analysis was about 33 million.

The SST k-ω model was used for the turbulence model. A fixed mass flow condition and a fixed static pressure condition were applied for inlet and outlet boundary conditions, respectively. Sliding boundary conditions were used between the rotating parts and stationary parts for transient analysis. The time step of the transient analysis was 1/360 of rotational speed (number of time steps for one rotation was 360). The pump performances and the thrust forces working on the impellers and the balance piston were calculated by using the time averaged values of pressure and velocity at two impeller rotation periods, after iterations for more than about ten impeller rotations

4. Pump performance and axial thrust characteristics

The pump performance is summarized by using non-dimensional forms, i.e. the flow coefficient ϕ, the head coefficient ψ, and the efficiency η ,which are defined as follows;

$$\phi = \frac{Q}{AU}, \quad \psi = \frac{gH}{U^2}, \quad \eta = \frac{\rho g Q H}{L} \tag{1}$$

where A (= $2\pi Rb$, b : impeller exit height) is the exit area of the impeller, U (= $R\omega$) is the impeller peripheral velocity, ρ is the density of water, and g is the gravitational acceleration. The pressure in the side wall gaps is defined by using the static pressure coefficient, which is defined as follows,

$$\psi_s = \frac{p - p_i}{0.5\rho U^2}, \quad (i = 1, 2). \tag{2}$$

The total axial thrust force F_A acting on the whole rotor is summarized by using a non-dimensional form as coefficient C_{F_A}, which is defined by

$$C_{F_A} = \frac{F_A}{\rho A U^2 / 2} \tag{3}$$

Figure 3. shows the measured and computed head coefficients and efficiencies of the three-stage pumps plotted against the flow coefficient. All the values are normalized by those at the design flow rate, ψ_d and η_d, for the nominal axial setup of $t/b = 0.0$.

The CFD results agree with the measured performances in general, although the CFD overestimated the head coefficient and efficiency at $\phi/\phi_d = 1.0$ (+2.6% in head, +5.6% in efficiency). Higher head and efficiency by CFD at $\phi/\phi_d = 1.0$ could be caused by ignoring the effects of the surface roughness of cast parts such as suction and discharge casings.

As shown in the figure, this pump shows a positive slope in the head curve near the shut-off condition. CFD predicted this feature, its flow rate, however, was slightly higher than in the experiment. The source of this head drop near the shut-off condition will be discussed later. Improvement of the accuracy of the CFD prediction at the part load condition is one of the challenges to overcome and should be achieved by using high-fidelity simulation, such as LES and DES or hybrid type turbulence simulations.

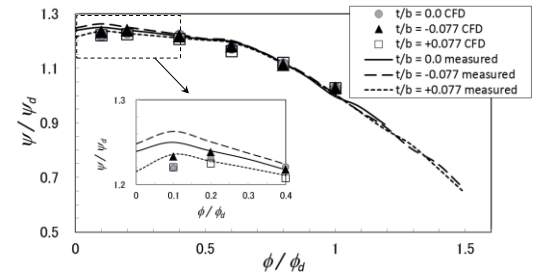

(a) Head coefficient

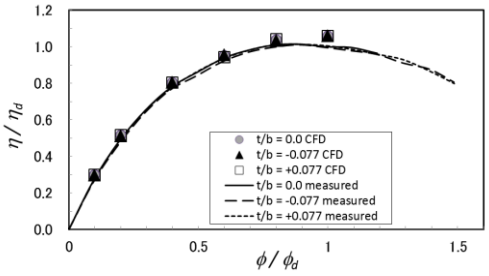

(b) Efficiency

Figure 3. Head characteristics of the three stages pump.

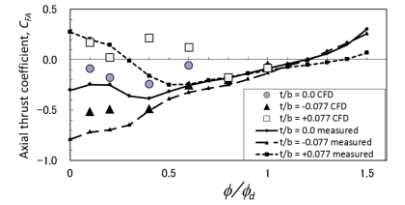

(a) Total thrust

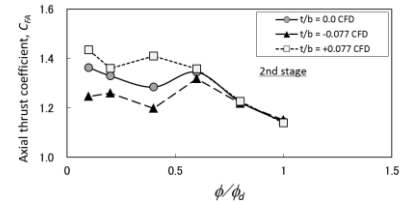

(b) 2nd stage impeller

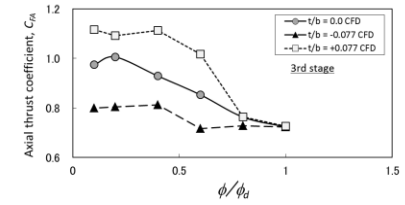

(c) 3rd stage impeller

Figure 4. Axial thrust characteristics.

Figure 4. (a) shows a comparison of the C_{F_A} calculated from the CFD results with the measurement values. The positive direction of the thrust is the direction from the discharge to the suction casing. The effects of pump rotor offsets on the axial thrust are clearly shown at the flow ratio ϕ/ϕ_d below 0.4 in the experimental results, while the CFD shows the effects at a higher flow at $\phi/\phi_d = 0.6$. With the negative rotor offset $t/b = -0.077$, the thrust force becomes negatively larger than that for $t/b = 0.0$, while the positive offset $t/b = +0.077$ reduces the thrust force.

Figure 4. (b) and figure 4. (c) show the C_{F_A} of the 2nd and 3rd stage impellers. The flow ratio start showing the effects of pump rotor offsets are different for 2nd and 3rd stage impellers: the flow is higher at $\phi/\phi_d = 0.6$ for 3rd stage impeller than 2nd stage impeller ($\phi/\phi_d = 0.4$). The difference in the flow ratio, where the effects of the pump rotor offsets to thrust force appear, is mainly caused by the 3rd stage impeller.

5. Interaction between the flow in the side wall gaps and reverse flow from diffuser

In order to clarify the source of discrepancy in thrust force characteristics between the experiments and CFD, changes in the interaction between the flow in the side wall gaps and reverse flow from the diffuser were investigated.

Figure 5 shows the locations of the planes on which the flow distribution are shown, placed at the impeller exit and gaps. First, the change in flow field in the diffuser and front side gap of the 3rd stage at a flow ratio of 1.0, 0.6 and 0.2 is shown in figure 6. This figure shows a radial velocity contour in the front side gap, velocity vectors near the shroud side of the diffuser, leakage flow in the clearance between the impeller and diffuser casing wall and flow in the gap. In the case of $\phi/\phi_d = 1.0$, flow in the diffuser is good without reverse flow. The flow in the diffuser channel stagnated and reverse flow developed at part of the channel at $\phi/\phi_d = 0.6$. The reverse flow flowing into the front side gap increased and its interaction with the gap flow became stronger, which, when evaluated by the inward flow, takes place in the gap (area of blue color in the radial velocity contour increased). One can see at $\phi/\phi_d = 0.2$, that the reverse flow developed more strongly and the interaction with the gap flow is much clearer.

Here, the calculated leakage flow ratio to the design flow is 4.0% at the front wearing ring, 2.3% at the inter-stage bush and 3.0 % at the balance piston at $\phi/\phi_d = 1.0$. In the case of $\phi/\phi_d = 0.1$, leakage flow ratio at the front wearing ring and balance piston is increased to 4.5% and 3.5% of the design flow, leakage flow ratio at the inter-stage clearance is almost the same as the value at $\phi/\phi_d = 1.0$.

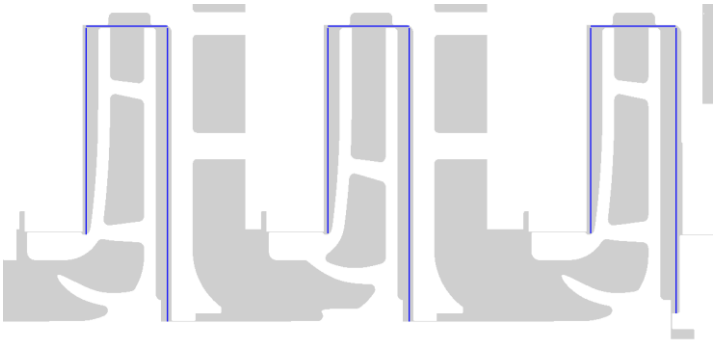

Figure 5. Locations of flow distribution at impeller exit and gaps.

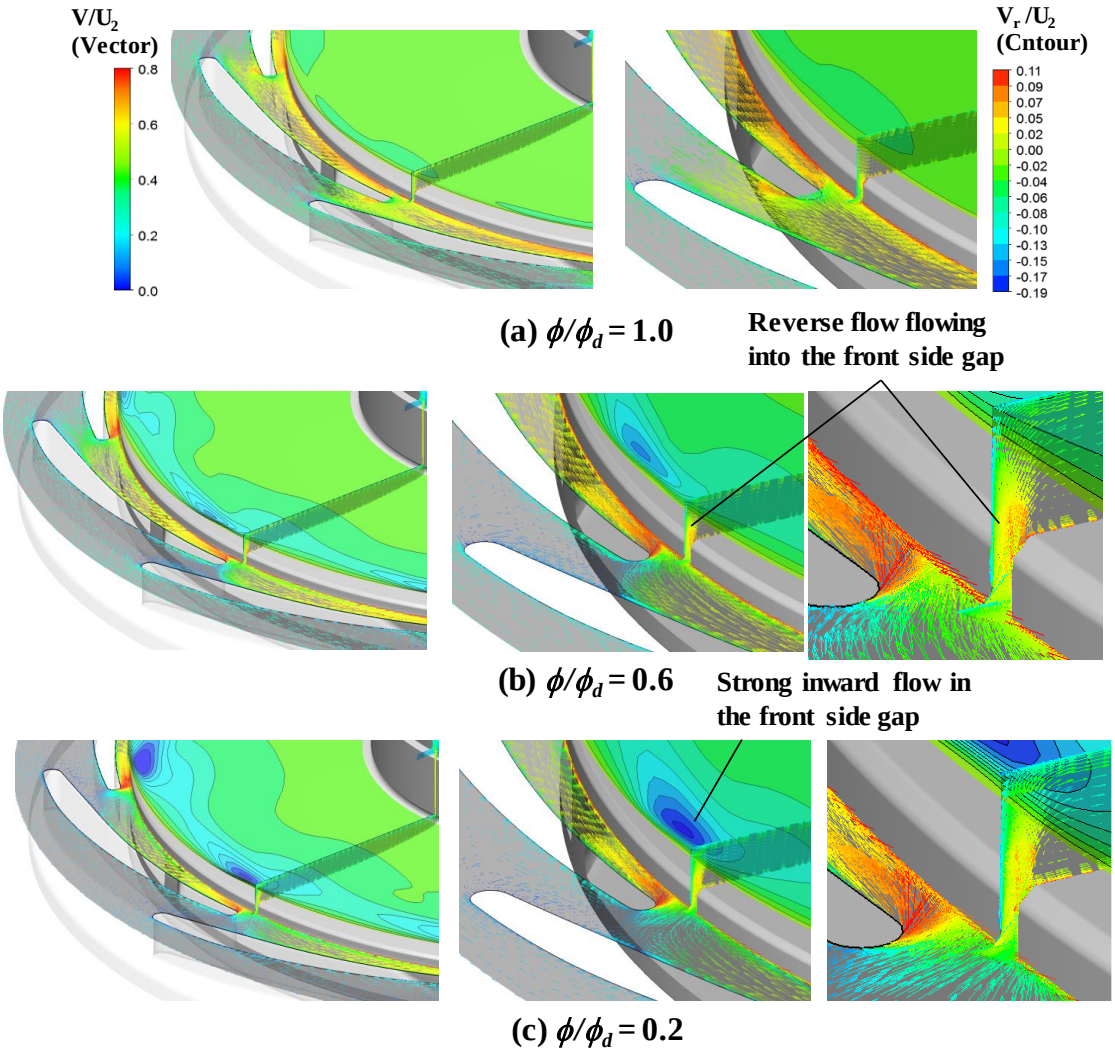

Figure 6. Velocity vector near the shroud side of diffuser and Vr contour in the front side gap (3rd stage, t/b = 0.0).

Figures 7. and figure 8. show the time averaged radial velocity distributions at the impeller exits and in the front and back side wall gaps of each impeller at $\phi/\phi_d = 0.6$, for all the axial offset cases ($t/b = 0.0$, $t/b = +0.077$, $t/b = -0.077$). The areas of strong inward flow in the gaps (blue areas of the radial velocity contour) developed more clearly in the 3rd stage than in the 1st and 2nd stages. The reason for the stronger inward flow in the gaps of the 3rd stage should be the stronger reverse flow in the diffuser of the 3rd stage than in that of 1st and 2nd stages with a smaller flow rate in the diffuser by the leakage flow to the balance piston.

In the case of $t/b = +0.077$, the rotor shifted to the suction side, a strong inward flow in the back side gap was developed, while in the case of $t/b = -0.077$, the rotor shifted to the discharge side, inward flow in the front side gap developed. These changes affect the pressure distributions in the gaps for each case.

Figure 9. shows the circumferentially and time averaged static pressure distributions at the front and back side gaps of the 3rd impeller. In the case of $t/b = +0.077$, the static pressure decreased in the front side gap and increased in the back side gap, which induced an increase of thrust force to the suction side. The inverse change happened in the case of $t/b = -0.077$. These changes are related closely to the swirl velocity distributions in the gaps shown in figure 10. The horizontal axis in the figure represents the swirl velocity factor $K = V_t/r\varpi$, where V_t is the circumferentially and time averaged swirl velocity, $r\varpi$ is local rotational velocity. The vertical axis represents the radius ratio, where r is radial location and R is the impeller outer radius. In the case of $t/b = +0.077$, the swirl velocity increased in the front side gap and decreased in the back side gap. This change was induced by the change in interactions between the reverse flow from the diffuser and the gap flows.

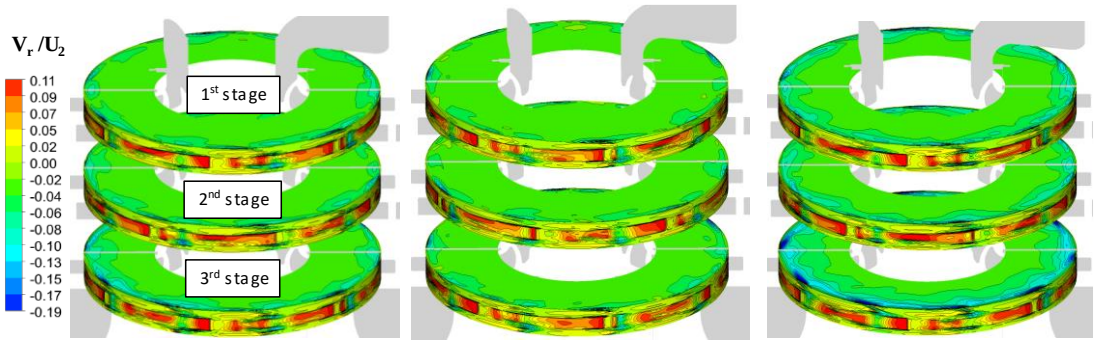

(a) t/b = 0.0 **(b) t/b = +0.077** **(c) t/b = -0.077**

Figure 7. Radial velocity distributions in the front sidewall gap and at the impeller exit ($\phi/\phi_d = 0.6$).

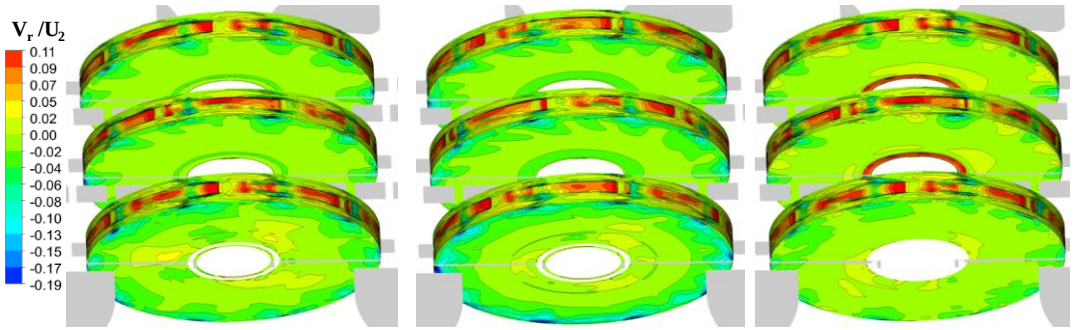

(a) t/b = 0.0 **(b) t/b = +0.077** **(c) t/b = -0.077**

Figure 8. Radial velocity distributions in the back sidewall gap and at the impeller exit ($\phi/\phi_d = 0.6$).

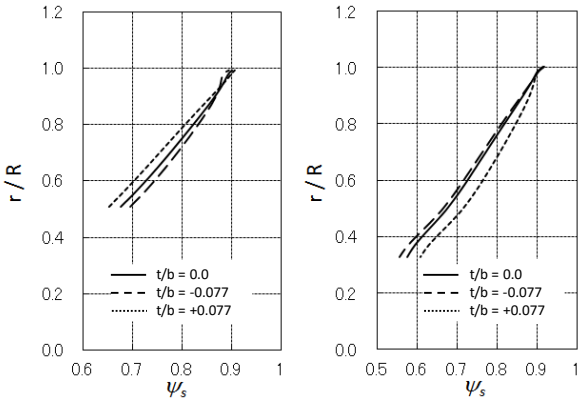

(a) In the front side gap (b) In the back side gap

Figure 9. Static pressure distributions in side wall gaps of the 3rd impeller (ϕ/ϕ_d = 0.6).

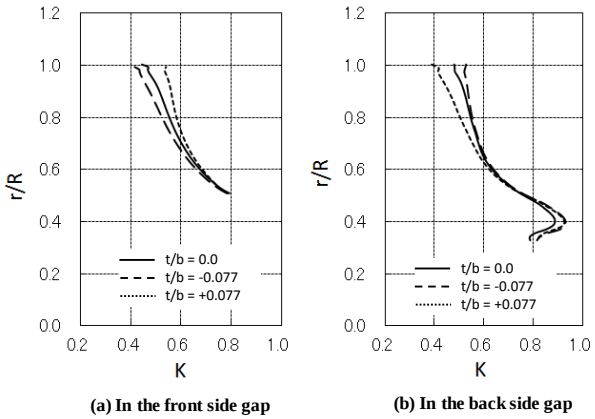

(a) In the front side gap (b) In the back side gap

Figure 10 Swirl velocity distributions in side wall gaps of the 3rd impeller (ϕ/ϕ_d = 0.6)

From the comparison between the experiments and CFD, it can be concluded CFD should overestimate the development of reverse flow in the diffuser and interactions between the reverse flow and flow in the gaps.

6. Relationship between flow field change and positive slope in head characteristic near the shut-off condition

In this section, the source of the positive slope in head characteristic near the shut-off condition will be discussed. CFD predicted head drop between the flow ratio of $\phi/\phi_d = 0.2$ to $\phi/\phi_d = 0.1$.

Figure 11. shows head and circumferential velocity at the inlet and exit of each impeller. In the calculation of these values, pressure and velocity only in the forward flow region were sampled and mass averaged at the part load condition. Under low flow conditions, reversed flow develops to large extent in the pump, especially between the impeller and the diffuser. In this case, the mass average will yield very large values because the sum of the mass flow at cross sections becomes small. To avoid this, a mass average was conducted at only the forward flow region. From figure 11. (a), one can see that each impeller shows a head drop at $\phi/\phi_d = 0.1$. Figure 11. (b) and figure 11. (c) show the effects of a decrease in UV_t at the impeller exit were essential to the positive slope in head characteristic near the shut-off condition.

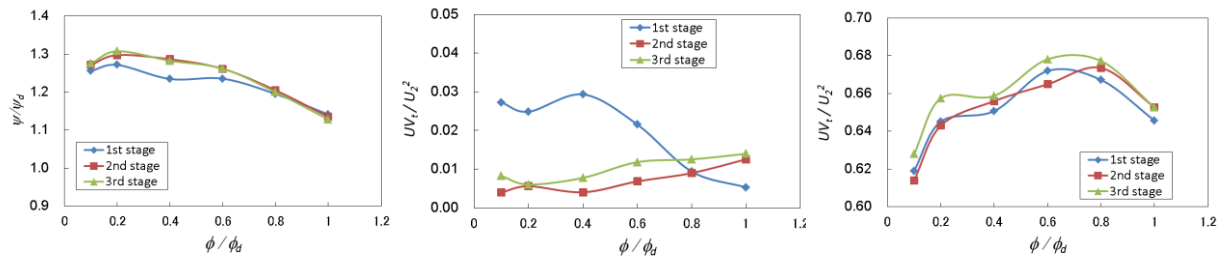

(a) Impeller head (b) Circumferencial velocity at impeller inlet (c) Circumferential velocity at impeller exit

Figure 11. Head and circumferential velocity at the inlet and exit of the impellers (t/b = +0.077).

Figure 12. shows reverse flow, relative velocity vectors near the 20% span and circumferential velocity distribution of the 3rd impeller. The inlet recirculation was already well developed at the $\phi/\phi_d = 0.4$. The size of the inlet recirculation region became slightly bigger at $\phi/\phi_d = 0.1$ and the effects on the UV_t at the impeller inlet were small, as shown in figure 11. (b). On the other hand, the recirculation region at the pressure side of the impeller blades developed toward the exit of the impeller and combined with the reverse flow from the downstream of the impeller (from the diffuser) at $\phi/\phi_d = 0.1$. At $\phi/\phi_d = 0.1$, the velocity vector diagrams also show the development of the reverse flow and accompanied passage vortex in the blade channels. These developments of reverse flow and passage vortex in the impeller should reinforce flow mixing and blockage of the flow and reduce V_t at the exit of the impeller, as shown by the contours downstream of the impeller.

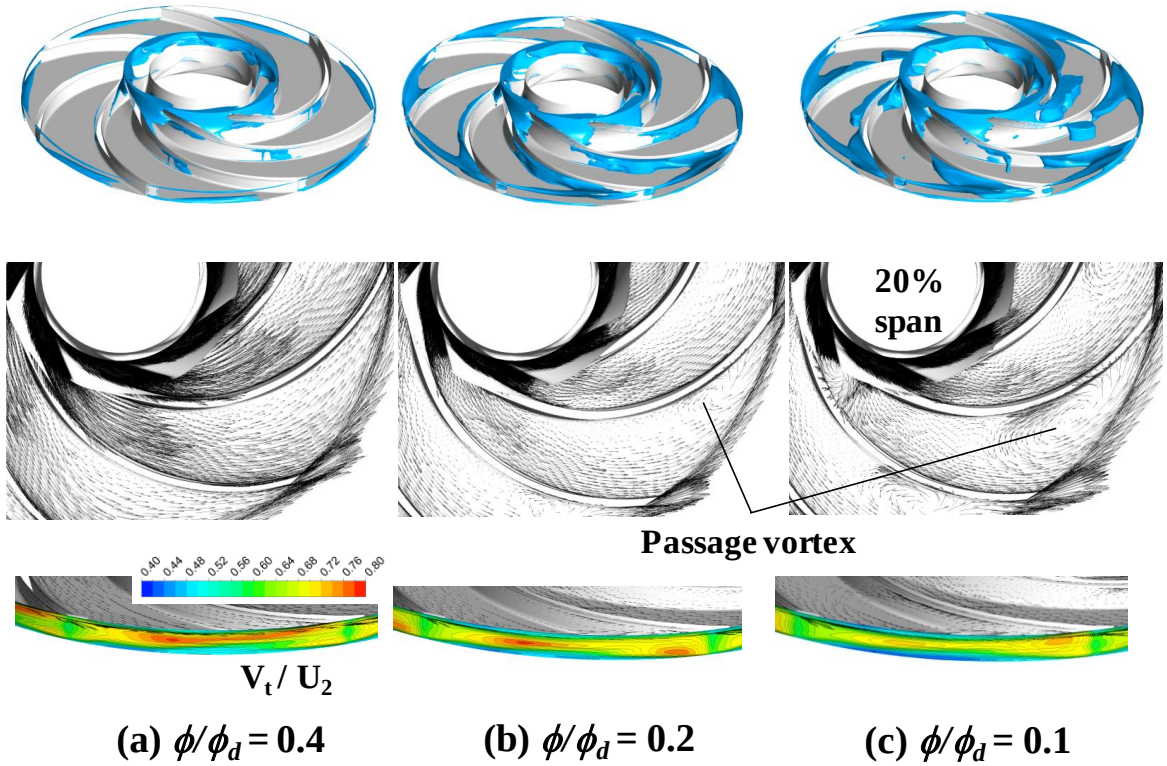

Figure 12. Reverse flow, relative velocity vectors and circumferential velocity distribution (3rd impeller).

7. Conclusions

This paper describes the results of URANS CFD prediction of performance, internal flow fields and thrust force acting on the impellers of a three-stage centrifugal pump which was provided for the Workshop "Single-&Multistage Pump Flow Prediction". The results of these investigations are as follows.

(1) The results of URANS CFD analysis of the three-stage centrifugal pump show good agreement with the measured results in pump head characteristic and efficiency at design and part load flow to $\phi/\phi_d = 0.1$.
(2) URANS CFD predictions on the thrust forces acting on the pump rotor near the design flow show good agreement with the measurement results. However, the URANS CFD predicted earlier change

in the axial thrust characteristic by axial shift of the rotor than the experiments yielded. This was caused by interaction between reverse flows and side wall gap flows starting at higher flow than in the experiments. It can be concluded that CFD overestimated the developments of reverse flow in the diffuser and interactions between the reverse flow and flow in the gaps.

(3) URANS predicted the positive slope in the head curve near the shut-off condition, its flow rate, however, was slightly higher than the experimental results. The positive slope in head curve near the shut-off condition should be caused by the developments of reverse flow and passage vortex in the impeller reinforcing flow mixing and blockage of the flow and reducing V_t at the exit of the impeller.

Acknowledgment

This study has been carried out as part of "HPC Project" and succeeding projects organized by Turbomachinary Society of JAPAN (TSJ), to provide the results of unsteady simulation of three-stage pumps by using URANS in Working Group 2 (WG2): Unsteady simulation of multi-stage centrifugal pump. The authors would like to express sincere gratitude to the members of WG2 for giving us the opportunity to take part in this study, as well as fruitful discussions throughout WG2 meetings. The author also would like to express his deepest appreciation to Professor Miyagawa and the staff and students of Miyagawa Lab of Waseda University for providing the hydraulic design of the test pump, and to Professor Watanabe and the staff and students of Kyusyu University for conducting many kinds of measurements. Finally, we would like to thank TSJ for organizing this project and DMW Corporation, Hitachi, Ltd., Mitsubishi Heavy Industries, Ltd., and Shin Nippon Machinery Co., Ltd., for their financial support during this project.

References

[1] Kurokawa, J., and Toyokura, T., 1972, "Study on Axial Thrust of Radial Flow Turbomachinery," Proceedings, The Second International JSME Symposium – Fluid Machinery and Fluidics, Tokyo, Japan, pp.31-40.

[2] Iino, T., Satp, H., and Miyashiro, H., 1980, "Hydraulic Axial Thrust in Multistage Centrifugal Pumps," ASME Journal of Fluids Engineering, 102, pp. 64-69.

[3] Salvadori, S., Della Gatta, S., Adami, P., Betolazzi, L., 2007, "Development of a CFD Procedure for the Axial Thrust Evaluation in Multistage Centrifugal Pumps," Proceedings of 7th European Conference on Turbomachinery.

[4] Bruurs, K.A.J., Van Esch, B.P.M., van Der School, M.S., van der Zijden, E.J.J., 2017, M., "Axial Thrust Prediction for a Multi-Stage Centrifugal Pump", Proceedings of the ASME 2017 Fluids Engineering Division Summer Meeting, FEDSM2017-69283.

[5] Hergt, P. and Starke, J., 1985, "Flow Patterns Causing Instabilities in the Performance Curves of Centrifugal Pumps with Vaned Diffusers," Proceedings of the Second International Pump Symposium, pp. 67-75.

[6] Thomae, H., and Stucki, R., 1970, "Axial Thrust Occuring in Multi-Stage Radial Pumps," Sulzer Technical Review.

[7] Watanabe, H., Yamashita, T., Watanabe, S., Hara, Y., 2015, "CFD Analysis of Axial Thrust in Three-Stage Centrifugal Pump at Design and Part Load Conditions," Proceesings of the ASME-JSME-KSME Joint Fluids Engineering Conference, AJK2015-33515.

[8] Yamashita, T., Watanabe, S., Hara, Y., Watanabe, H., 2015, "Measurement of Axial and Radial Thrust Forces Working on a Three-Stage Centrifugal Pump Rotor," Proceesings of the ASME-JSME-KSME Joint Fluids Engineering Conference, AJK2015-33515.

[9] ANSYS, Inc., ANSYS CFX-Solver Theory Guide, ANSYS CFX Release 14.0, (2013).